

See discussions, stats, and author profiles for this publication at: <https://www.researchgate.net/publication/371481067>

Assessing Cement Matrix Permeability by Neutron Dark Field Imaging

Chapter · June 2023

DOI: 10.1007/978-3-031-33211-1_31

CITATIONS

0

READS

36

8 authors, including:



Luca Valentini

University of Padova

92 PUBLICATIONS 1,325 CITATIONS

[SEE PROFILE](#)



Gregorio Dal Sasso

Italian National Research Council

31 PUBLICATIONS 598 CITATIONS

[SEE PROFILE](#)



Matteo Busi

Paul Scherrer Institut

24 PUBLICATIONS 136 CITATIONS

[SEE PROFILE](#)



Giorgio Ferrari

Mapei SpA

51 PUBLICATIONS 830 CITATIONS

[SEE PROFILE](#)

Some of the authors of this publication are also working on these related projects:




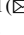






Alpine Archaeocopper Project AAcP [View project](#)



Zeolites: Mineralogy, Crystal Structure, Crystal Chemistry [View project](#)



Assessing Cement Matrix Permeability by Neutron Dark Field Imaging

Luca Valentini¹  , Gregorio dal Sasso² , Fabio Castiglioni³ , Matteo Busi⁴ ,
Giorgio Ferrari³, Maria Chiara Dalconi¹ , Markus Strobl⁴ , and Gilberto Artioli¹ 

¹ University of Padua, Padua, Italy
luca.valentini@unipd.it

² National Research Council - Institute of Geosciences and Georesources, Padua, Italy

³ Mapei SpA, Milan, Italy

⁴ Paul Scherrer Institut, Villigen, Switzerland

Abstract. The permeability of hardened cement plays a crucial role in determining the durability of cement-based materials. In this contribution, we explore a novel approach to the study of small-scale porosity in cement pastes, and how its modification can affect the overall permeability. Experiments based on neutron dark-field imaging (BOA beamline – Paul Scherrer Institut) were designed with the aim of achieving a detailed and quantitative description of the pore structure in cement pastes. Paste and mortar samples were prepared with a water-to-cement ratio of 0.45. After curing in wet conditions, all samples were cut in slices of different thickness (2, 4, 6, 8 and 10 mm) to evaluate optimal neutron transmission conditions. Correlation length plots obtained from the dark field imaging signals are aimed to provide quantitative information on the pore network topology, which in turn controls the permeability of cement-based materials. This technique was preliminary implemented to the characterization of changes occurring within the pore network, in the presence of admixtures based on Cu-doped C-S-H nanocomposites, which were shown to induce a modification in the mechanism of C-S-H nucleation, promoting both an acceleration of early hydration kinetics and a reduction in permeability.

Keywords: Dark field imaging · Neutrons · Permeability · C-S-H · Nucleation

1 Introduction

The pore network topology of hardened cement determines the permeability of the matrix of cement-based materials, which in turn plays a fundamental role in controlling durability.

The use of calcium-silicate-hydrate (C-S-H) and transition metal silicate hydrate (Me-S-H) synthetic nanoparticles as seeding agents in cement has a direct impact on the kinetics of dissolution/precipitation during the hydration process, promoting C-S-H precipitation in the pore space (rather than at the surface of unhydrated cement particles) and accelerating the overall hydration process [1]. Other than enhancing early strength

development, it has been observed that the switch from heterogeneous (i.e. controlled by foreign substrates) to secondary (i.e. controlled by pre-existing substrates of the nucleating phase) nucleation, occurring in the presence of C-S-H nanoparticles, induces a decrease in the permeability of the hardened matrix [2].

In this contribution, we aim at reconciling the macroscopic observation of reduced permeability in the presence of a Cu-doped C-S-H nanocomposite admixture (Me-S-H), with microscopic details of the pore network topology, assessed by means of neutron dark-field imaging.

2 Preliminary Assessment of the Me-S-H Nanocomposite and its Effect

The used nanocomposite consists of a colloidal suspension of Cu-doped C-S-H nanoparticles (Fig. 1), stabilised by means of PCE polymers. The nanocrystalline structure (Fig. 1) was characterised by combining small-angle X-ray Scattering (SAXS) and synchrotron wide-angle X-ray total scattering (WAXS) [3].

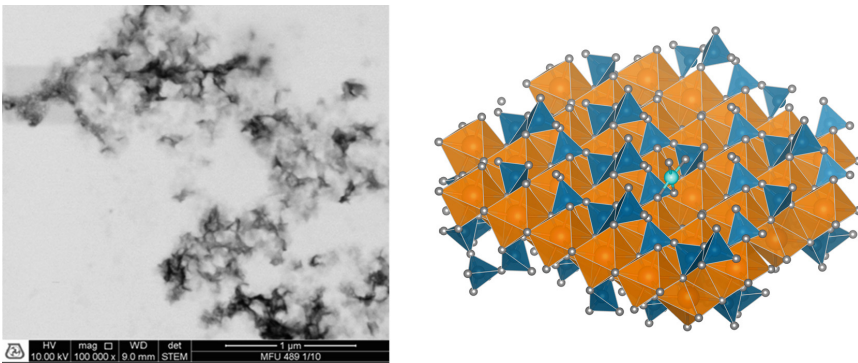


Fig. 1. TEM image of Me-S-H nanoparticle aggregates present in the admixture used in this study (left). Structure of the Cu-doped C-S-H nanoparticles (right); orange = Ca coordination polyhedra; blue = Si tetrahedra; cyan = copper

To assess the action of the nanocomposite, all tests were performed using CEM III/A 42.5R cement, with the addition of 2.66% Me-S-H admixture. Further information on the physical and chemical properties of the admixture is provided elsewhere [2].

Tests performed on concrete, according to EN 12,390-8 [4], showed an 8% reduction of water penetration in the presence of the admixture. Furthermore, chloride ingress and carbonation depth were also reduced [5].

Switching from the macroscopic to the microscopic scale of observation, ionic diffusion through the cement matrix was tracked by an X-ray imaging method that monitors the penetration of a potassium iodide solution (acting as a contrast medium to enhance the visualization of the permeation front), with micrometre resolution [6]. Cement pastes, in the absence and presence of the Me-S-H nanocomposite, were molded in prismatic

cuvettes of $1 \times 1 \times 4.3 \text{ cm}^3$ size and cured for 28 days at $23 \text{ }^\circ\text{C}$ and 95% RH. At the end of the curing period, 1 mL of KI solution was placed on the upper surface of each sample, which was subsequently irradiated by a W-anode X-ray beam with 100 kV energy. X-ray attenuation images were acquired for 24 h, with 1 h interval. The results displayed in Fig. 2 demonstrate a slower kinetics of ionic diffusion in the presence of the admixture.

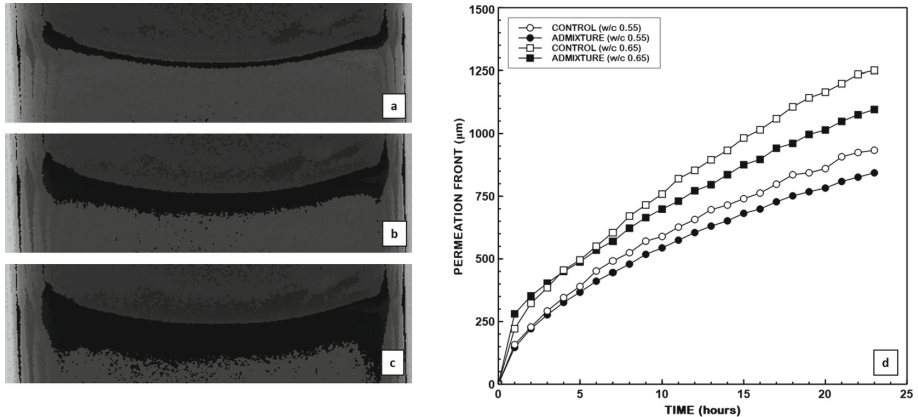


Fig. 2. X-ray images of the ion diffusion front, in the presence of the Me-S-H admixture, at 1 (a), 6 (b) and 12 (c) hours of contact with the KI solution. Plots of the extent of the ion diffusion front obtained from the X-ray images, for samples prepared with w/c 0.55 and 0.65, in the absence and in the presence of the Me-S-H admixture

3 Neutron Dark Field Imaging

Neutron grating interferometry (nGI) [7] was implemented to the study of the changes in pore network topology occurring in the presence of the Me-S-H nanocomposite. The experiments were carried out at BOA (Beamline for neutron Optics and other Approaches) [8], SINQ (Paul Scherrer Institut).

The setup (Fig. 3) consists of a source absorption grating (G0) that forms coherent neutron beamlets. The second grating (G1) induces phase shift of the neutron beam array, with formation of an interference pattern, dependent on the period of G1 and the wavelength of the neutron beam. The analysing absorption grating (G2) is placed in proximity of the detector and has the same period of the interference pattern, allowing it to be resolved. To obtain the interference pattern at each pixel of the detector, a phase-stepping approach is used by translating G0 across the beam. Further details of the method and specific instrumental setup are reported elsewhere [9]. This technique provides both the transmission image, forming by attenuation of neutrons, and the dark-field image (DFI), due to small-angle neutron scattering (SANS) interactions. Spatial resolution in transmission mode is limited by the imaging geometry and intrinsic resolution of the detector. On the other hand, DFI can provide insight into structural heterogeneities

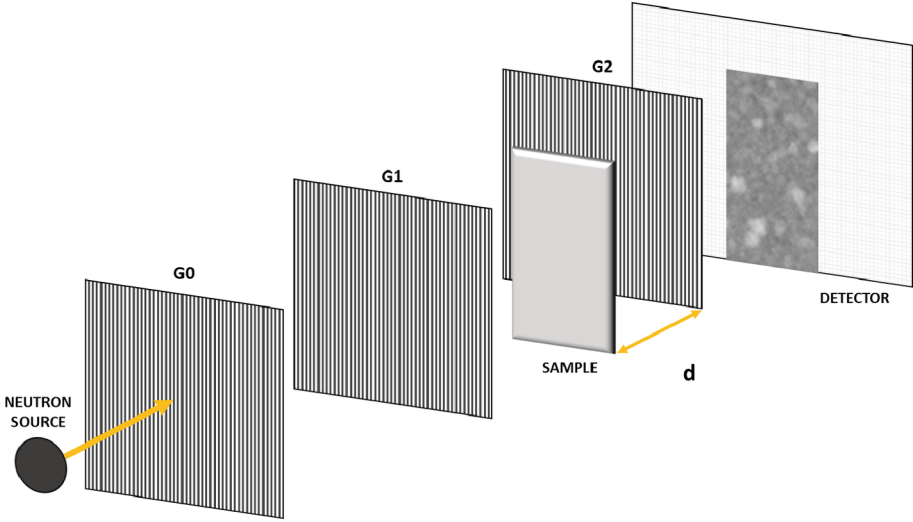


Fig. 3. Sketch of the experimental setup. The neutron grating interferometer is constituted by: a source absorption grating (G0) that induces the formation of coherent beamlets; a phase grating (G1) that generates an interference pattern (*Talbot carpet*); an analysing absorption grating (G2) placed in proximity of the detector. The samples are mounted on a linear stage able to translate the sample at a distance d from the G2 grating, defining the autocorrelation length probed

between a few hundreds of nanometres and a few micrometres. The intensity variation of the interference pattern is measured in each pixel in the absence of the sample, then the change in visibility is measured when the sample is placed between G1 and G2, giving the dark field imaging signal:

$$DFI(\xi) = \exp[\Sigma_s t (G(\xi) - 1)] \quad (1)$$

where ξ is the auto-correlation length, Σ_s is the SANS macroscopic cross section (1/length dimension), t is the sample thickness, G is the correlation function (dimensionless) describing the scattering structure of the sample, as a function of the auto-correlation length. The probed length scale is given by:

$$\xi = \lambda d / p \quad (2)$$

where λ is the neutron wavelength, d the distance between sample and G2 grating (Fig. 3) and p the period of the gratings in a Talbot-Lau interferometer setup. The effect of structural heterogeneities present in the sample over different auto-correlation lengths can then be probed.

3.1 Sample Preparation

Both paste and mortar samples were used for the nGI measurements. Paste samples were prepared using CEM-III/A and deionised water ($w/c = 0.45$). Mortars were prepared as the paste samples, with addition of quartz sand. After curing for 28 days at ambient

temperature and 95% RH, the samples were cut in slices of different thickness (from 2 to 10 mm), with the aim of defining the optimal level of image contrast, and dried overnight at 50 °C. Before performing the measurements, each set of samples was stored in the following different conditions, in an attempt of optimising the output signal: a) dry conditions; b) immersed in H₂O for 2 days; c) immersed in H₂O for 4 days; d) immersed in D₂O for 2 days.

Figure 4 displays neutron attenuation images for mortar samples (2 days in H₂O) with different thickness. The 2 mm sample was chosen for the next experiments, as the one providing optimal contrast, without excessive neutron attenuation.

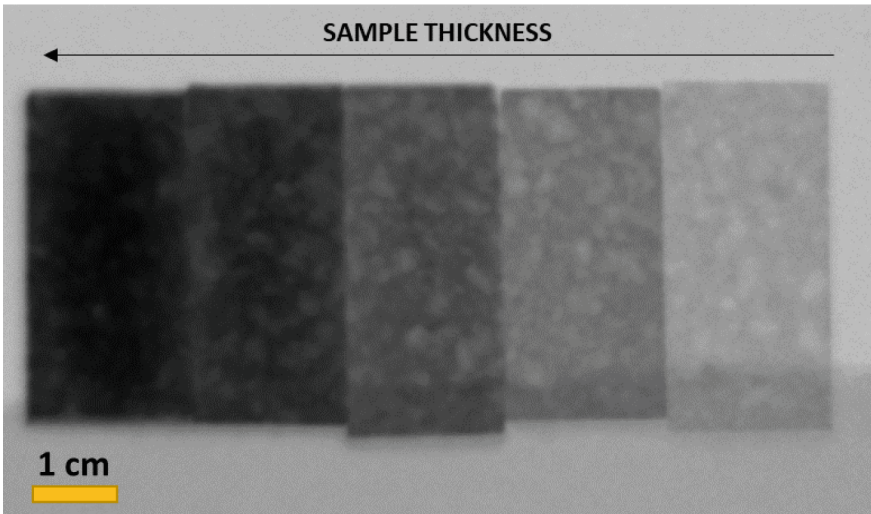


Fig. 4. Neutron attenuation images for samples having (right to left) 2, 4, 6, 8 and 10 mm thickness

3.2 DFI Image Analysis

Example DFI images for paste samples with different storage conditions, in the absence and in the presence of the Me-S-H admixture, are displayed in Fig. 5.

Qualitatively, the two samples stored in H₂O display stronger DFI contrast, as compared to: a) samples stored in dry conditions, because of (partial) evaporation of H₂O and hence less neutron scattering from hydrogen nuclei; b) samples stored in D₂O, because of lower scattering cross section of deuterium compared to protium.

A step towards quantitative characterisation [10] was performed by plotting the DFI value vs. probed auto-correlation length (Fig. 6), with the aim of assessing possible variations in the presence of the Me-S-H nanocomposite admixture. The autocorrelation length provides information on how water-filled pores of a given size are correlated in space.

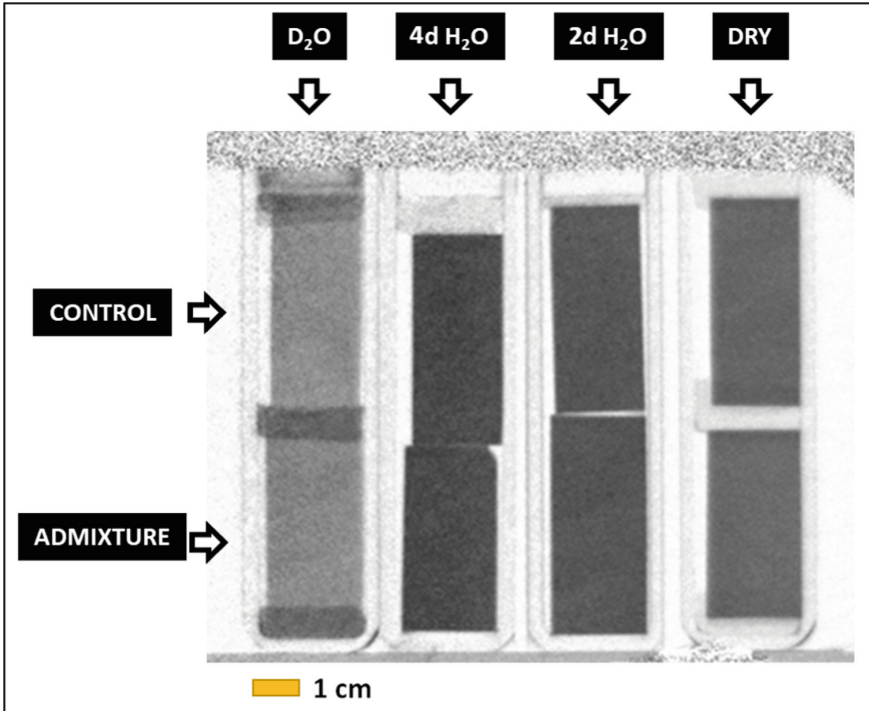


Fig. 5. DFI images for paste samples at 740 nm auto-correlation length

4 Discussion and Conclusions

The curves in Fig. 6 display significant variations of the DFI contrast with the auto-correlation length, when samples stored in different modes are compared. The relative extents of DFI values measured are: $D_2O > dry > 2 \text{ days } H_2O > 4 \text{ days } H_2O$, which was expected because of the larger scattering cross section of the protium isotope as compared to deuterium. This means that the DFI contrast is proportional to the amount of H_2O in the pore network. The observation that the DFI value for the sample stored in dry condition is lower than the one stored in D_2O , suggests that a certain amount of H_2O remained in the pore network, even if the sample was not immersed in water prior to the measurement.

When comparing pairs of samples, stored under the same conditions, with and without the addition of nanoparticles, minor differences are observed. A relative decrease of the DFI value in admixed samples is observed when the overall amount of water is decreased (from dry conditions to storage in H_2O for 4 days). For the samples stored in D_2O , a lower DFI value is observed for the admixed sample. In general, no significant changes in slope with correlation length were observed. Such a change would be expected in the presence of a pore refinement mechanism, associated with a change in nucleation mechanism, which would explain the observed permeability reduction when the Me-S-H nanocomposite is added to the mix.

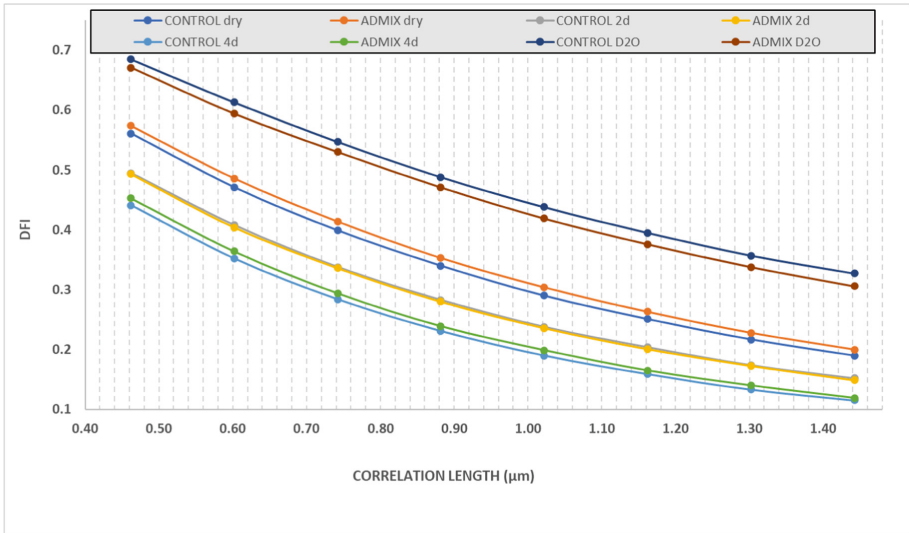


Fig. 6. DFI vs. auto-correlation length plots for paste samples stored in different conditions, in the absence and in the presence of the Me-S-H nanocomposite admixture

One possibility is that adequate auto-correlation length ranges were not probed during the set of experiments performed.

To better assess the effect of the Me-S-H nanocomposite on the pore network topology at small scale, we plan to perform further experiments, in which different auto-correlation length values and the effect of different curing regimes will be investigated. Furthermore, we plan to carry out a more quantitative analysis of the experimental data, by modelling the correlation function G (Eq. 1) according to different structural configurations.

In conclusion, dark field imaging based on neutron grating interferometry may represent a promising approach to the study of fine details of the pore network topology in cement matrices. In this study, we performed some preliminary experiments by which we could fine-tune some details of sample preparation and experimental setup. Further experimenting and modelling approach to data analysis will be necessary to extract more accurate information, aimed at reconciling the small-scale properties of the pore network with macroscopic properties that control the durability of cement-based materials.

References

1. Artioli, G., Ferrari, G., Dalconi, M.C., Valentini, L.: Nanoseeds as modifiers of the cement hydration kinetics. In: Liew, M.S., Nguyen-Tri, P., Nguyen, T.A., Kakooei, S. (eds.) *Smart Nanoconcretes and Cement-Based Materials*, pp. 257–269. Elsevier (2020)
2. Valentini, L., Ferrari, G., Russo, V., et al.: Use of nanocomposites as permeability reducing admixtures. *J. Am. Ceram. Soc.* **101**, 4275–4284 (2018)
3. Dal Sasso, G., Dalconi, M.C., Ferrari, G., et al.: An atomistic model describing the structure and morphology of Cu-doped C-S-H hardening accelerator nanoparticles. *Nanomaterials* **12**, 342 (2022)

4. EN 12390-8: Testing hardened concrete – part 8: depth of penetration of water under pressure (2019)
5. Artioli, G., Bravo, A., Broggio, S., et al.: Low-carbon durable concrete for the new Genoa's San Giorgio bridge. *ACI Spec. Publ.* **SP-355**, 1–10 (2022)
6. Moradillo, M.K., Hu, Q., Ley, M.T.: Using X-ray imaging to investigate in-situ ion diffusion in cementitious materials. *Constr. Build. Mater.* **136**, 88–98 (2017)
7. Strobl, M., Grunzweig, C., Hilger, A., et al.: Neutron dark-field tomography. *Phys. Rev. Lett.* **101**, 123902 (2008)
8. Morgano, M., Peetermans, S., Lehmann, E.H., et al.: Neutron imaging options at the BOA beamline at Paul Scherrer Institut. *Nuclear Instrum. Methods Phys. Res. Sect. A: Accel. Spectrom. Detect. Assoc. Equip.* **754**, 46–56 (2014)
9. Kim, Y., Valsecchi, J., Kim, J., et al.: Symmetric Talbot-Lau neutron grating interferometry and incoherent scattering correction for quantitative dark-field imaging. *Sci. Rep.* **9**, 18973 (2019)
10. Strobl, M.: General solution for quantitative dark-field contrast imaging with grating interferometers. *Sci. Rep.* **4**, 7243 (2014)